Neutron Diffraction Studies of Fluid Bilayers with Transmembrane Proteins: Structural Consequences of the Achondroplasia Mutation

Xue Han,* Mihaela Mihailescu,† and Kalina Hristova*
*Department of Materials Science and Engineering, Johns Hopkins University, Baltimore, Maryland; and †Department of Physiology and Biophysics, University of California, Irvine, California

ABSTRACT Achondroplasia, the most common form of human dwarfism, is due to a G380R mutation in the transmembrane domain of fibroblast growth factor receptor 3 (FGFR3) in >97% of the studied cases. While the molecular mechanism of pathology induction is under debate, the structural consequences of the mutation have not been studied. Here we use neutron diffraction to determine the disposition of FGFR3 transmembrane domain in fluid lipid bilayers, and investigate whether the G380R mutation affects the topology of the protein in the bilayer. Our results demonstrate that, in a model system, the G380R mutation induces a shift in the segment that is embedded in the membrane. The center of the hydrocarbon core-embedded segment in the mutant is close to the midpoint between R380 and R397, supporting previous measurements of arginine insertion energetics into the endoplasmic reticulum. The presented results further our knowledge about basic amino-acid insertion into bilayers, and may lead to new insights into the mechanism of pathogenesis in achondroplasia.

INTRODUCTION

Hydropathy plot analysis is widely used to identify membrane-embedded segments in membrane proteins and predict membrane protein topologies (1,2). Usually, a prediction is considered correct if there is an overlap between the known and the predicted transmembrane (TM) helices, irrespective of the exact helix length (3). Predictions of exact hydrocarbon core-embedded sequences, however, are rarely correct. Furthermore, recent work by Hessa et al. (4,5) has demonstrated that for some amino acids, particularly hydrophilic charged ones, the free energy of partitioning into the membrane depends strongly on the position of the amino acid within the bilayer thickness. The observed positional dependence is not yet incorporated into hydropathy prediction tools, and thus the identification of exact hydrocarbon core-embedded segments is a challenge. The need therefore remains to experimentally determine transmembrane segments, by measuring the depth of penetration of specific amino acids within the bilayer thickness.

Two methods, fluorescence quenching (6–8) and electron paramagnetic resonance (EPR) spectroscopy (9–12), are often used to obtain the depth of penetration of a specific amino-acid residue of a protein into the bilayer. A ''reporter molecule,'' such as a fluorophore or an EPR probe, is attached to a specific cysteine in the protein, and the experiments ''locate the reporter'' within the bilayer thickness. The precision in determining the depth of penetration using these two methods is 1.5–3 Å.

Neutron diffraction experiments, combined with specific deuteration of amino acids of interest (13–16), can offer some advantages over the methods of EPR and fluorescence quenching. First, diffraction gives direct structural information (as opposed to, say, fluorescence, where we measure the fluorescence signal, and infer structure from the signal). Second, the experimental resolution of diffraction experiments can be very high, ~0.2 Å (17). Third, in a diffraction experiment we can obtain and compare structural characteristics with and without the label and thus determine if the protein disposition and the overall structure of the bilayer changes in the presence of the label. This is not an option for either EPR or fluorescence, where the signal is present only in the presence of the label.

In neutron diffraction experiments, contrast is introduced by selective deuteration of amino acids. Although hydrogen-deuterium substitutions in membrane proteins are expected to not perturb the structure of the proteins in the bilayer and the structure of the bilayer itself, the lack of such perturbations has not been demonstrated explicitly. Furthermore, it is not known if the selective deuteration of an amino acid provides sufficient contrast, such that the depth of penetration of the label can be determined reliably using neutron diffraction.

Here we explore the feasibility of determining depth of penetration of amino acids in transmembrane domains using neutron diffraction. We use the methodology to obtain structural information about the naturally occurring transmembrane domain sequence of human fibroblast growth factor receptor 3 (FGFR3). FGFR3 is a receptor tyrosine kinase that conducts biochemical signals via lateral dimerization in the membrane plane. It consists of an extracellular ligand binding domain, a single TM domain, and a cytoplasmic catalytic domain, and the TM domain has been shown to play an important role in the signal transduction process (18,19).

In our laboratory, we study the biophysics behind defects in FGFR3 signaling due to pathogenic mutations in the TM

Submitted June 26, 2006, and accepted for publication August 17, 2006.

Address reprint requests to K. Hristova, Tel.: 410-516-8939; E-mail: kh@jhu.edu.

0006-3495/06/11/3736/12 $2.00

doi: 10.1529/biophysj.106.092247

domain (20–22). These mutations have been identified in genetic studies of patients afflicted by growth disorders and cancers (23,24), but the effect of these mutations on protein-protein and protein-lipid interactions are not well understood.

An example of a pathogenic FGFR3 TM mutation is the G380R mutation linked to achondroplasia, the most common form of human dwarfism, in >97% of all studied cases (24,25). While receptor tyrosine kinase TM domain mutations are generally believed to induce pathologies by stabilizing the active dimeric state of the receptors (26,27), the molecular mechanism behind achondroplasia is under debate and different mechanisms may contribute to the induction of the phenotype (22,28–30). From a structural perspective, it is intriguing that the mutation introduces an arginine in the middle of the predicted TM domain of the protein. Arginine is rarely found in the bilayer hydrocarbon core, and it is possible that the G380R substitution induces a shift in the membrane-embedded segment of the protein; such a shift may be the structural basis of pathogenesis in achondroplasia.

The hydropathy plot prediction of the membrane-embedded FGFR3 segment, carried out using Membrane Protein Explorer (http://blanco.biomol.uci.edu/mpex/), suggests that the TM domains of wild-type and mutant are the same, with R380 inserted in the bilayer (22) (see Fig. 1). R380 is surrounded by very hydrophobic amino acids, and such prediction is not surprising. Hessa et al. (4), however, have demonstrated a strong dependence of the penalty for inserting arginine on its depth of penetration into the hydrocarbon core; this penalty is the highest in the middle of the bilayer. Thus, it is unlikely that the location of R380 within the bilayer, and the topology of the mutant TM domain, can be predicted accurately with current hydropathy plot algorithms that do not take into account the observed positional dependence.

The neutron diffraction structural methods, used here to study the topology of the wild-type FGFR3 TM domain and the achondroplasia-causing mutant, are based on the analysis of the so-called ''absolute, or per-lipid'' structure factors (31–33). These absolute structure factors are determined by the scattering of the unit cell, and do not depend on the exact experimental conditions such as amount of sample in the beam, precise geometry, etc. The absolute scale methodology has previously provided valuable information about the structure of fluid bilayers, such as the complete structure of the DOPC bilayer (34) and the position of amphipathic helices within the bilayer interface (35,36). Now we extend this methodology to determine the depth of penetration of amino acids in the fluid bilayer, as well as the topology of the FGFR3 TM domain in the bilayer.

Here we show that the depth of penetration of amino acids into the hydrocarbon core can indeed be determined using neutron diffraction. The results from the diffraction experiments, together with oriented circular dichroism (OCD) measurements of FGFR3 helix tilt in bilayers, can be used to identify the membrane-embedded segment of the R380 FGFR3 mutant. We find that R380 in the mutant is located at ~11 Å from the bilayer center, within the hydrocarbon core of the bilayer. We further find that the G380R mutation induces a shift in the hydrocarbon core- embedded segment of the protein. The presented structural work furthers our knowledge about basic amino-acid insertion into bilayers, and addresses, for the first time, the structural consequences of the achondroplasia mutation.

MATERIALS AND METHODS

Sample preparation

1-Palmitoyl-2-oleoyl-*sn*-glycero-3-phosphocholine (POPC) was purchased from Avanti Polar Lipids (Alabaster, AL), D_2O from Cambridge Isotope Labs (Andover, MA), amino acids from Advanced Chemtech (Louisville, KY), and deuterated amino acids (Phe, Leu, Val) from CDN isotope (Pointe-Claire, Quebec). Peptide synthesis details were reported previously (37). Multilayer samples containing 4 mol % TM_{wt}, $TM_{wt}^{D(FL)}$, TM_{mut}, $TM_{mut}^{D(FL)}$, and $TM_{mut}^{D(LVV)}$ (see Fig. 1 for sequences) were prepared by dissolving the peptides in a mixture of trifluoroethanol and hexafluoroisopropanol (2:1 ratio) and the lipid (POPC) in chloroform (38,39). The two solutions were mixed in the appropriate ratios and deposited on a thin glass slide, which was followed by the gradual and complete evaporation of the solvents. The multilayer sample size was ~15 mm × 17 mm × 0.5 μm.

Oriented CD

The above method was also used to prepare samples for oriented circular dichroism (OCD) measurements, such that neutron and OCD results can be directly compared. A multilayer sample was deposited on a quartz slide. The

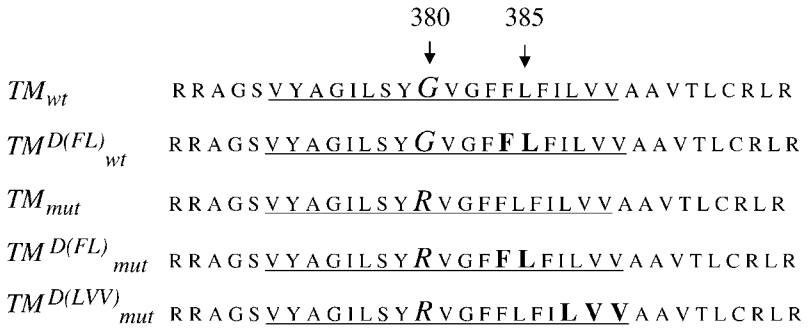

FIGURE 1 Amino-acid sequences of the five human FGFR3 TM domain variants studied here, with the predicted hydrocarbon core-embedded segments underlined. Hydropathy plot predictions were carried out using Membrane Protein Explorer, a Java applet available over the WWW (http://blanco.biomol.uci.edu/mpex/). The deuterated amino acids are shown in bold. The G380R mutation (*italic*) has been linked to achondroplasia, the most common form of dwarfism in humans.

slide was placed in a custom-designed chamber with the multilayers perpendicular to the beam (35,36,40–42). To hydrate at 76% relative humidity (RH), a drop of saturated NaCl solution was placed in the chamber and the sample was equilibrated for several hours (32,36). The sample was rotated around the beam axis in increments of 45°, such that eight spectra were recorded for each sample. The spectra shown in Fig. 2 were obtained after averaging and lipid background corrections.

Neutron diffraction experiments, data collection and analysis

Neutron diffraction experiments were performed at the Advanced Neutron Diffractometer/Reflectometer at the National Institute of Standards and Technology Center for Neutron Research (Gaithersburg, MD). Relative humidity of 76% was achieved using a saturated NaCl solution, as previously described (32). Each multilayer sample was hydrated using H_2O mixed with 0%, 20%, and 50% D_2O. The solution was placed next to the sample in a sealed aluminum container, and diffraction pattern changes were followed during sample equilibration. Typically, 6~7 h were needed for complete equilibration.

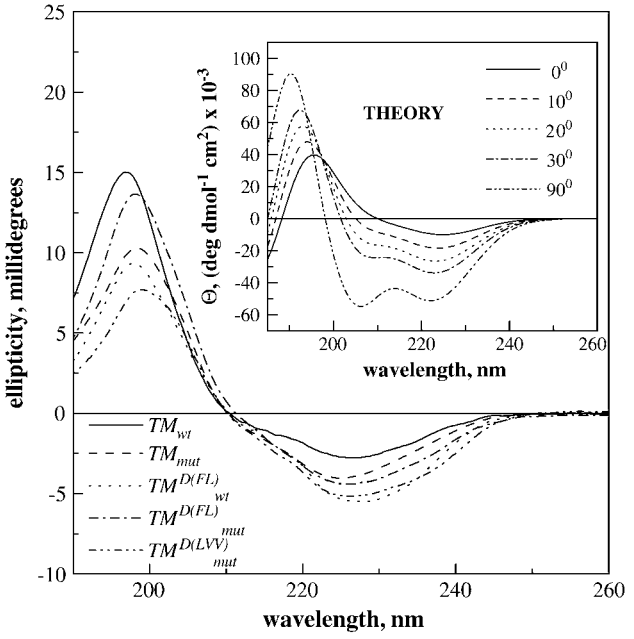

FIGURE 2 Oriented CD spectra of 4 mol % TM_{wt}, $TM_{wt}^{D(FL)}$, TM_{mut}, $TM_{mut}^{D(FL)}$, and $TM_{mut}^{D(LVV)}$ in POPC multilayers equilibrated at 76% RH. Peptides and lipids (molar ratio 1:24) were mixed in HFIP/TFE/chloroform, deposited on a quartz slide, and hydrated to form multilayers. The experimental spectra are compared to theoretical spectra of helices (*inset*) with tilts of 0° (*solid line*), 10° (*dashed line*), 20° (*dotted line*), 30° (*dashed dotted line*), and 90° (*dashed dotted-dotted line*) with respect to the bilayer normal. The theory predicts that tilts of 20° and higher will result in the appearance of a minimum at ~205 nm (*inset*). The OCD signal of a TM helix is very low and challenging to measure above the lipid background, particularly at lower wavelengths, and the amplitude of the signal depends on the thickness of the sample, which is hard to control. Thus, the observed difference in amplitude in the experimental spectra is not statistically significant (22,37). Based on the shape of the experimental data, showing no defined peak at 205 nm, it appears that all peptides are transmembrane and their tilt with respect to the bilayer normal is 20° or less.

The wavelength of the neutron beam was 5 Å. The intensity of the diffracted beam was recorded during Θ–2Θ scans using an He-3 gas-filled 25.4-mm-wide pencil detector (GE Reuter-Stokes, Twinsburg, OH). Data processing was performed using Reflred, a software written for the Advanced Neutron Diffractometer/Reflectometer, and the commercially available package Origin (OriginLab, Northampton, MA).

The observed structure factors were calculated as

$$f(h) = \sqrt{I(h)A(h)\sin(2\Theta)}, \tag{1}$$

where $I(h)$ is the intensity of the h^{th} peak, $A(h)$ is the absorption correction, and $\sin(2\Theta)$ is the Lorentz factor. The absorption correction is given by (43)

$$A(h) = \frac{\sin\Theta}{2\mu t}[1 - \exp^{-2\mu t/\sin\Theta}], \tag{2}$$

where Θ is the Bragg angle, t is the sample thickness, and μ is the linear absorption coefficient of the sample. In all cases, $A(h)$ did not exceed 1.005, such that the absorption correction was negligible.

Absolute scaling

The absolute scattering length density $\rho^*(z)$ is the scattering density per one lipid molecule, given by (33)

$$\rho^*(z) = \rho(z)S = \rho_0^* + \frac{2}{d}\frac{1}{\bar{k}}\sum_{h=1}^{h_{obs}} f(h)\cos\left(\frac{2\pi hz}{d}\right), \tag{3}$$

where $f(h)$ are the measured structure factors on an arbitrary scale, $\bar{k}$ is the instrumental constant, d is the Bragg spacing, ρ_0^* is the average scattering length density of the unit cell, and h_{obs} is the highest observed diffraction order. $F(h) = f(h)/\bar{k}$ are the absolute structure factors, which are determined solely by the structure and the scattering of the unit cell (17,32).

The instrumental constant $\bar{k}$ and the absolute structure factors $F(h) = f(h)/\bar{k}$ can be determined if diffraction patterns are recorded for two samples, with unit cells which are identical except for a few atoms that have large differences in scattering lengths (i.e., isomorphous unit cells). Here the absolute scale profiles were determined by comparing structure factors for POPC bilayers containing 4 mol % TM_{wt} and $TM_{wt}^{D(FL)}$, 4 mol % TM_{mut} and $TM_{mut}^{D(FL)}$, and 4 mol % TM_{mut} and $TM_{mut}^{D(LVV)}$, as discussed below.

The $D(FL)$ and $D(LVV)$ deuterium labels introduce only 0.625 and 1.08 deuterons per lipid, respectively (see Results, below). Large random errors in the experimental structure factors can ''obscure'' the contrast provided by the deuterium label. The random errors in the experimental structure factors were therefore minimized by placing the structure factors for each peptide on a self-consistent arbitrary scale and linearizing them with D_2O concentration, as described previously (17,32). The four sets of structure factors $\{f_0(h), f_{20}(h)$, and $f_{50}(h)\}$, recorded for 100% H_2O, 20% H_2O + 80% D_2O, and 50% H_2O + 50% D_2O hydration, are linear with D_2O concentration, thus demonstrating that the D_2O/H_2O replacement is isomorphous (see Fig. 3). Therefore, the following relation holds for structure factors of a particular multilayer sample collected at 0, 20, and 50% D_2O (17),

$$\frac{f_{20}(h)}{k_{20}} = 0.6\frac{f_0(h)}{k_0} + 0.4\frac{f_{50}(h)}{k_{50}}, \tag{4}$$

where k_0, k_{20}, and k_{50} are self-consistent, yet arbitrary instrumental constants for 100% H_2O, 20% H_2O + 80% D_2O, and 50% H_2O + 50% D_2O, respectively. The linear relationship (4) can be used to find the self-consistent arbitrary instrumental constants and the ''best'' statistical estimates of the observed structure factors $\{\bar{f}_0(h), \bar{f}_{20}(h)$, and $\bar{f}_{50}(h)\}$ from parameters of the best-fit straight lines passing through the experimental structure factors (see further details in (17,32)).

Next, the best estimates of the experimental structure factors $\bar{f}_0^{wt}(h)$, $\bar{f}_0^{wt\_D}(h)$, $\bar{f}_0^{mut}(h)$, and $\bar{f}_0^{mut\_D}(h)$, recorded for 100% H_2O, were used to obtain the instrumental constants needed to place these structure factors on the absolute scale, using

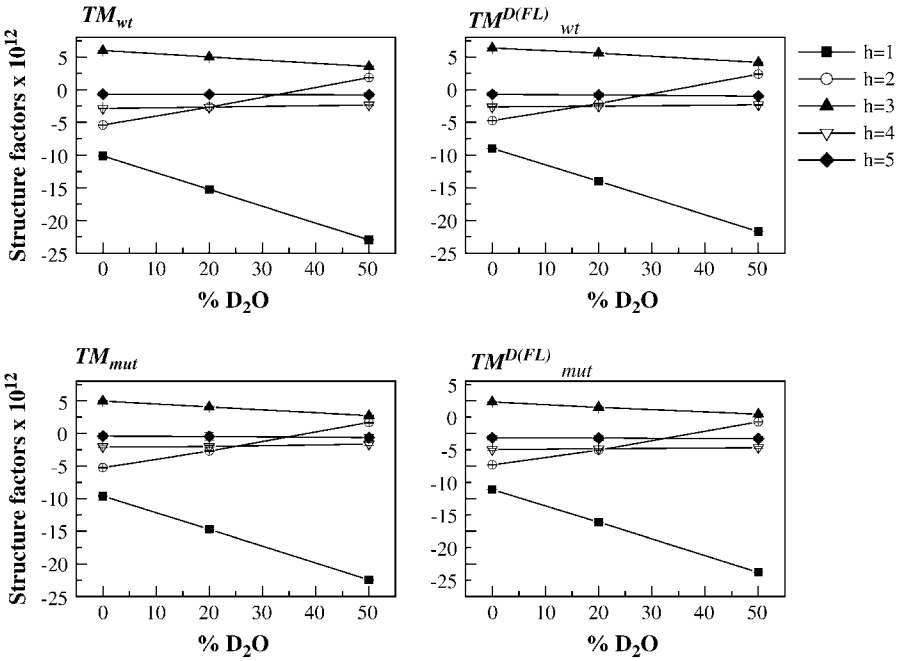

FIGURE 3 Observed structure factors for POPC multilayers containing 4 mol % TM_{wt}, $TM_{wt}^{D(FL)}$, TM_{mut}, and $TM_{mut}^{D(FL)}$, equilibrated at 76% RH, as a function of D_2O mol %. The structure factors have been placed on the absolute (per lipid) scale, as described in Materials and Methods. The experimental uncertainties have been calculated as described in the text. The linear dependence of the structure factors on D_2O mol % demonstrates that the H_2O/D_2O exchange is an isomorphous replacement. These plots can be used to determine the signs of the structure factors (Table 1), as previously described (17,32).

$$\frac{\bar{f}_0^{\mathrm{wt\_D}}(h)}{\bar{k}_0^{\mathrm{wt\_D}}} - \frac{\bar{f}_0^{\mathrm{wt}}(h)}{\bar{k}_0^{\mathrm{wt}}} = 2b_{\mathrm{D}}\exp\left(-\left[\pi A_{\mathrm{D}}^{\mathrm{wt}}h/d\right]^2\right) \cos(2\pi h Z_{\mathrm{D}}^{\mathrm{wt}}/d),\ h = 1 \ldots . h_{\mathrm{obs}}, \quad (5)$$

$$\frac{\bar{f}_0^{\mathrm{mut\_D}}(h)}{\bar{k}_0^{\mathrm{mut\_D}}} - \frac{\bar{f}_0^{\mathrm{mut}}(h)}{\bar{k}_0^{\mathrm{mut}}} = 2b_{\mathrm{D}}\exp\left(-\left[\pi A_{\mathrm{D}}^{\mathrm{mut}}h/d\right]^2\right) \cos(2\pi h Z_{\mathrm{D}}^{\mathrm{mut}}/d),\ h = 1 \ldots . h_{\mathrm{obs}}. \quad (6)$$

Here A_D and Z_D are the width and the position of the peptide deuterium label, either $D(FL)$ or $D(LVV)$, that we would like to determine for the wild-type and the mutant, $\{\bar{k}_0\}$ are the instrumental constants, and b_D is the neutron scattering length difference due to the hydrogen/deuterium substitution in the peptide. Five orders of diffraction were recorded in all experiments, such that $h_{obs} = 5$. Therefore, the overdetermined system of five expressions (Eq. 5) can be used to find the four unknown parameters for wild-type: $\bar{k}_0^{wt}$, $\bar{k}_0^{wt\_D}$, A_D^{wt}, Z_D^{wt}. The other five sets of expressions (Eq. 6) are used to calculate the four unknown parameters for mutant: $\bar{k}_0^{mut}$, $\bar{k}_0^{mut\_D}$, A_D^{mut}, Z_D^{mut}.

Knowing the instrumental constants $\bar{k}_0$, we can now determine the absolute structure factors for 100% H_2O, $F_0^{wt}(h) = (\bar{f}_0^{wt}(h)/\bar{k}_0^{wt})$, $F_0^{wt\_D}(h) = (\bar{f}_0^{wt\_D}(h)/\bar{k}_0^{wt})$, $F_0^{mut}(h) = (\bar{f}_0^{mut}(h)/\bar{k}_0^{mut})$, and $F_0^{mut\_D}(h) = (\bar{f}_0^{mut\_D}(h)/\bar{k}_0^{mut})$, as well as their best estimates $\overline{F}_0^{wt}(h) = (\bar{f}_0^{wt}(h)/\bar{k}_0^{wt})$, $\overline{F}_0^{wt\_D}(h) = (\bar{f}_0^{wt\_D}(h)/\bar{k}_0^{wt\_D})$, $\overline{F}_0^{mut}(h) = (\bar{f}_0^{mut}(h)/\bar{k}_0^{mut})$, and $\overline{F}_0^{mut\_D}(h) = (\bar{f}_0^{mut\_D}(h)/\bar{k}_0^{mut\_D})$. Next, we find the instrumental constants for the structure factors collected at 20% and 50% D_2O, according to

$$\frac{\bar{f}_\xi(h)}{\bar{k}_\xi} - \overline{F}_0 = 2b_{\mathrm{w}}N_{\mathrm{w}}\xi\exp\left(-\left[\pi A_{\mathrm{w}}h/d\right]^2\right) \cos(2\pi h Z_{\mathrm{w}}/d),\ h = 1 \ldots . h_{\mathrm{obs}}, \quad (7)$$

where ξ is the D_2O fraction (either 20% or 50%), N_w is the number of water molecules per lipid, and b_w is the neutron scattering length difference between H_2O and D_2O. The four unknowns, to be calculated from the overdetermined system of five expressions (Eq. 7), are the parameters of the water distribution A_w, Z_w, and N_w, and the instrumental constant. Finding the set of instrumental constants $\bar{k}_\xi$ allows us to determine the absolute structure factors $F_\xi(h) = f_\xi(h)/\bar{k}_\xi$ and their best estimates $\overline{F_\xi}(h) = \overline{f_\xi}(h)/\bar{k}_\xi$ for $\xi =$ 20% or 50%.

Error analysis

The experimental errors in the structure factors $\sigma(h)$ were determined from the square roots of the integrated peak areas and the background below the peaks, as described previously (*32*;*35*). The quality of the neutron data was described by the so-called self R-factor, $R_{self} = \sum_{h=1}^{h_{obs}} \sigma(h) / \sum_{h=1}^{h_{obs}} F(h)$ (35). The value of R_{self} was compared to $R_{diff} = \sum_{h=1}^{h_{obs}} \Delta F(h) / \sum_{h=1}^{h_{obs}} F(h)$, where $\Delta F(h)$ are the difference structure factors due to the deuterium label. The position of the label can be determined and the structure factors can be scaled only if the changes in the structure factors due to the label are larger than the random noise in the structure factors, i.e., if $R_{diff} > R_{self}$. The values of R_{diff} are given in Table 2, and R_{self} values are given in Table 1. In all cases, $R_{diff} > R_{self}$.

R-factors of fits were calculated according to $R_{fit} = \sum_{h=1}^{h_{obs}} |(F - F_{fit})(h)| / \sum_{h=1}^{h_{obs}} |F(h)|$, where F_{fit} are the calculated structure factors for the optimal position and width of the deuterium label. A fit was considered good if $R_{fit} < R_{self}$. Values for R_{fit} are shown in Tables 2 and 3 for the peptide label and the water distributions, respectively. In all cases, $R_{fit} < R_{self}$, indicative of good fits.

RESULTS

Direct determination of depth of penetration of amino acids in a fluid bilayer

Peptides corresponding to the wild-type and mutant FGFR3 TM domains (TM_{wt} and TM_{mut}, and deuterated variants, see Fig. 1) were produced by solid phase peptide synthesis (37). Solid-phase peptide synthesis is uniquely suited for introducing deuterated amino acids of choice into any sequence. A question arises, however, about the deuterium detection limit in neutron diffraction experiments (i.e., the number of deuterons per lipid that can be detected), as determined by the number of deuterons per peptide and the peptide/lipid ratio. Preliminary experiments, monitoring changes in structure factors as a function of D_2O content in the hydrating atmosphere (unpublished results), were used to estimate the

number of deuterons per lipid that can be easily detected. We observed that the introduction of 0.54 deuterons per lipid led to modest, but measurable changes in structure factors (data not shown). We therefore hypothesized that at least ~0.5 deuterons per lipid are required to provide sufficient contrast, and we designed the experiments such that the concentration of the deuterium exceeds this limit. We synthesized wild-type and mutant FGFR3 TM domain variants with deuterated F384 and L385, thus introducing 15 deuterons per peptide (referred to as ''*D*(*FL*) label''). The incorporation of 4 mol % of these peptides into POPC multilayers ensured the presence of 0.625 deuterons per lipid.

Overall, we synthesized four different peptides: TM_{wt}, $TM_{wt}^{D(FL)}$, TM_{mut}, and $TM_{mut}^{D(FL)}$ (see Fig. 1), following the published synthesis protocol (37). The molecular weights of the synthesized peptides, determined using MALDI-TOF mass spectrometry, matched exactly the calculated ones. Multilamellar POPC samples with 4 mol % of each peptide were prepared as described in Materials and Methods. All four peptides adopted transmembrane orientation in the POPC multilayers characterized by low tilt (<20°) with respect to the bilayer normal. The tilt was measured using oriented CD (OCD), as described in Materials and Methods (see comparison of experimental and theoretical OCD spectra in Fig. 2). The multilayer samples were placed in the neutron beam and equilibrated at 76% RH (32). Diffraction patterns were recorded at the Advanced Neutron Diffractometer/Reflectometer at the National Institute of Standards and Technology Center for Neutron Research.

The major goal of the neutron diffraction experiments was to measure the transbilayer distribution of the deuterium label *D*(*FL*) in bilayers containing either the wild-type or the mutant FGFR3 TM domain. To compare the neutron scattering length density profiles of different samples, the profiles were scaled and placed on the so-called absolute-scale. Absolute profiles have been discussed in detail previously (17,31,32), and the scaling protocol is given in Materials and Methods. The absolute structure factors for POPC bilayers with 4 mol % TM_{wt}, $TM_{wt}^{D(FL)}$, TM_{mut}, and $TM_{mut}^{D(FL)}$, together with the measured Bragg spacings, are shown in Table 1 for 100% H_2O. The absolute structure factors, as a function of D_2O content, are plotted in Fig. 3. The calculated absolute scattering length density profiles, obtained using Eq. 3, are shown in Fig. 4 for 0%, 20%, and 50% D_2O.

The direct comparison of the absolute wild-type profiles in Fig. 5 reveals the position of the deuterated amino acids within the bilayer thickness. Fig. 5 *A* compares the profiles of POPC bilayers with 4 mol % TM_{wt} (*solid line*) and 4 mol % $TM_{wt}^{D(FL)}$ (*dashed line*), hydrated in 100% H_2O. The obvious difference between the two wild-type profiles in the proximity of the bilayer center is due to the exchange of 15 hydrogens with deuterons in amino acids F384 and L385. The profiles overlap in the region away from the label, indicating that the hydrogen/deuterium exchange in F384/L385 constitutes an isomorphous replacement.

The experimental difference profile for wild-type, obtained by subtracting the POPC/TM_{wt} profile from the POPC/$TM_{wt}^{D(FL)}$ profile, is shown in Fig. 5 *B* (also in Fig. 5 *C*) with the thick dotted line. The difference profile is the transbilayer F384/L385 deuterium distribution *D*(*FL*), which can be deconvoluted into two symmetric Gaussian distributions with centers $\pm Z_{D(FL)}$ and width $A_{D(FL)}$, as described in Materials and Methods. The center of the fitted Gaussian distribution gives the position, $\pm Z_{D(FL)}$, of the *D*(*FL*) label. Note that the insertion of the peptide is not unidirectional, but symmetric, which gives rise to two symmetric label distributions around the bilayer center.

The quality of the fit in Fig. 5 was judged by the value of $R_{fit} = \sum_{h=1}^{h_{obs}} |(F - F_{fit})(h)| / \sum_{h=1}^{h_{obs}} |F(h)|$, where $F(h)$ indicates the experimental structure factors and $F_{fit}(h)$ indicates the calculated structure factors for a particular Gaussian position and width pair, $Z_{D(FL)}$ and $A_{D(FL)}$ (35). A fit was considered good if $R_{fit} < R_{self}$, where R_{self} describes the quality of the experimental data (see Error Analysis in Materials and Methods and Table 1). We found that, for wild-type, a range of positions and widths (i.e., multiple fits) are consistent with the experimental data, as illustrated in Fig. 5, *B* and *C*. For all these fits, $R_{fit} < R_{self}$. In Fig. 5 *B*, $Z_{D(FL)} = 0.2$ Å and $A_{D(FL)} = 5.8$ Å, and in Fig. 5 *C*, $Z_{D(FL)} = 2.4$ Å and $A_{D(FL)} = 4.3$ Å. The individual F384/L385 Gaussians are shown with dashed lines; their envelopes (*solid line*) approximate well the experimental profile (*thick dotted line*). The parameters of the Gaussian distributions for wild-type, consistent with the data ($R_{fit} < R_{self}$), are $0 \le Z_{D(FL)} \le 2.5$ Å and $4 \le A_{D(FL)} \le 5.8$ Å. Exact values of $Z_{D(FL)}$ and $A_{D(FL)}$ cannot be

TABLE 1 Observed absolute structure factors and their experimental uncertainties for POPC multilayers with 4 mol % peptide

*h**	TM_{wt}	$TM_{wt}^{D(FL)}$	TM_{mut}	$TM_{mut}^{D(FL)}$	$TM_{mut}^{D(LVV)}$
1	−10.13 ± 0.02	−8.98 ± 0.03	−9.62 ± 0.03	−8.60 ± 0.03	−7.66 ± 0.05
2	−5.40 ± 0.04	−4.73 ± 0.04	−5.24 ± 0.05	−4.83 ± 0.04	−4.57 ± 0.08
3	6.03 ± 0.04	6.40 ± 0.05	4.94 ± 0.07	4.80 ± 0.06	5.20 ± 0.11
4	−2.87 ± 0.07	−2.62 ± 0.08	−2.06 ± 0.13	−2.47 ± 0.11	−2.08 ± 0.25
5	−0.66 ± 0.27	−0.68 ± 0.30	−0.43 ± 0.44	−0.69 ± 0.35	−0.47 ± 0.48
R_{self}†	0.017	0.021	0.033	0.028	0.049
d (Å)‡	49.6 ± 0.1	49.4 ± 0.2	48.4 ± 0.3	48.3 ± 0.2	48.8 ± 0.2

*Diffraction order.
†Self *R*-factor, $R_{self} = \sum_{h=1}^{h_{obs}} |\sigma(h)| / \sum_{h=1}^{h_{obs}} |F(h)|$, describing the quality of the experimental data.
‡Bragg spacing.

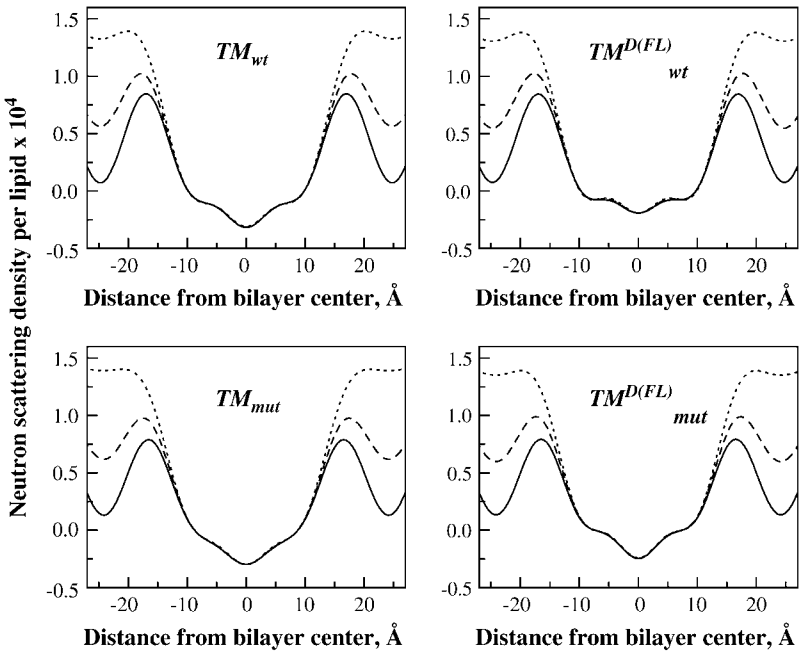

FIGURE 4 Absolute neutron scattering length density profiles of POPC bilayers with 4 mol % TM_{wt}, $TM_{wt}^{D(FL)}$, TM_{mut}, and $TM_{mut}^{D(FL)}$. Profiles are shown for 0% D_2O (*solid lines*), 20% D_2O (*dashed lines*), and 50% D_2O (*dotted lines*). Profiles were generated using Eq. 3 and the ''best'' absolute structure factors (see Materials and Methods). The differences between the profiles, due to the isomorphous H_2O/D_2O replacement, report the overlapping water distributions of apposing bilayers (see also Fig. 7).

calculated because the label is very close to the bilayer center and the two Gaussians overlap.

The position of the *D*(*FL*) deuterium label at $0 \leq Z_{D(FL)} \leq 2.5$ Å in wild-type suggests that the two labeled amino acids, F384 and L385, are very close to the bilayer center. Therefore, the hydropathy analysis prediction that V381 is in the middle of the bilayer (Fig. 1), and thus the F384/L385 label is at ~5 Å from the bilayer center, is not consistent with the experimental data.

Similarly to wild-type, the position of the *D*(*FL*) label in the R380 mutant can be determined by comparing the absolute scattering density profiles of bilayers containing the mutant peptides TM_{mut} and $TM_{mut}^{D(FL)}$ (Fig. 6), in the presence and absence of the *D*(*FL*) label. Fig. 6 *A* compares the profiles of bilayers with 4 mol % TM_{mut} and $TM_{mut}^{D(FL)}$, hydrated in 100% H_2O. Just as in Fig. 5 *A*, the difference between the two profiles is due to the isomorphous replacement of 15 hydrogens with deuterons in F384 and L385. Fig. 6 *B* shows the experimental difference profile for the mutant (*thick dotted line*), obtained by subtracting the two profiles shown in Fig. 6 *A*. In this case, the exact position and width of the F384/L385 deuterium distribution can be reliably determined as $Z_{D(FL)} = 4.6 \pm 0.2$ Å, $A_{D(FL)} = 3.8 \pm 0.2$ Å; $R_{fit} < R_{self}$ is satisfied for these values only. Exact values can be obtained because the label is not too close to the bilayer center and the overlap of the two Gaussians is lower than in the wild-type case. The individual F384/L385 Gaussians in Fig. 6 *B* are shown with dashed lines; the solid line is their envelope.

The water distribution

Data collection for various H_2O/D_2O ratios serves several purposes, provided that the H_2O/D_2O substitution is an isomorphous replacement. First, it allows us to reduce the random noise in the experimental data (17,32). Second, it allows us to determine the phases of the structure factors, as described in detail elsewhere (17,32). Third, it allows us to directly determine the distribution of the water, uptaken by the bilayer (31).

The H_2O/D_2O substitution is indeed an isomorphous replacement for all samples that we examined, as evident from the following observations: 1), the measured Bragg spacings do not depend on the D_2O mol fraction; 2), the dependence of the structure factors on D_2O content in Fig. 3 is linear; and 3), the profiles in Fig. 4, calculated for 0% D_2O (*solid line*), 20% D_2O (*dashed line*), and 50% D_2O (*dotted line*), overlap completely outside the water region. Thus, the profiles in Fig. 4 can be used to probe the hydration of the bilayers with wild-type and mutant proteins. The difference profiles in Fig. 7, obtained by subtracting the 0% D_2O profiles from the 20% D_2O profiles, report the transbilayer distribution of the water molecules, uptaken by bilayers containing wild-type and mutant FGFR3 TM domains.

While the hydration of the lipid multilayers has been determined as 6.2 waters per lipid at 76% RH (32), the uptake of water by the bilayer changes in the presence of the peptides (35). The scaling algorithm described in Materials and Methods allows the determination of the unknown hydration. By fitting Gaussians to the experimental difference profiles, we determine the center and the width of the water distribution, as well as the number of water molecules per lipid (Eq. 7). The parameters of the water distributions for bilayers containing wild-type and mutant TM domains are presented in Table 3. The fitted water Gaussians are shown in Fig. 7 with the dashed lines. The solid lines in Fig. 7, which closely follow the experimental profiles (*thick*

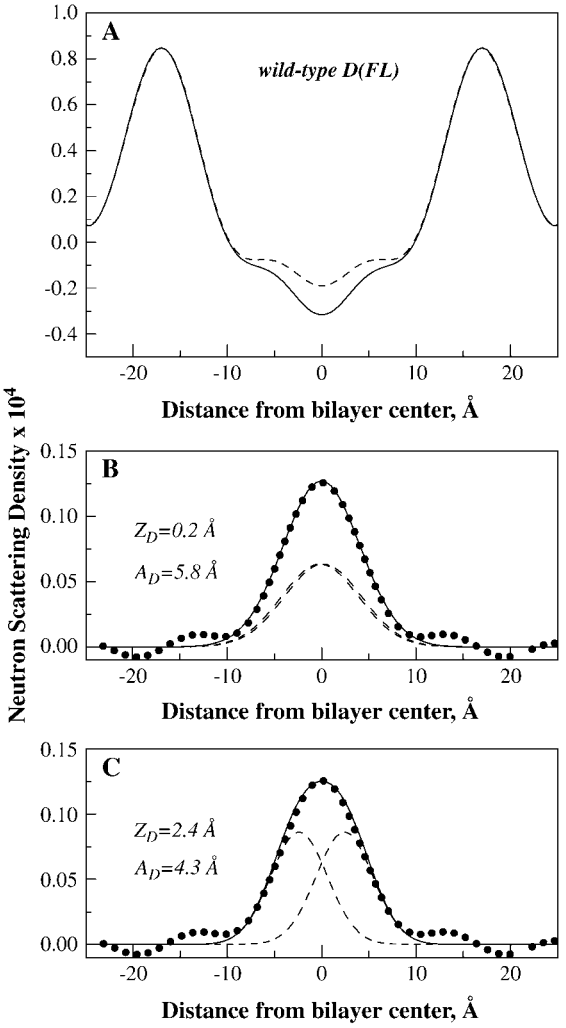

FIGURE 5 (*A*) Absolute neutron scattering length density profiles for bilayers with 4 mol % TM_{wt} and $TM_{wt}^{D(FL)}$. The obvious difference between the two profiles is due to the isomorphous replacement of 15 hydrogens in F384 and L385 with 15 deuterons (see Fig. 1). (*B*,*C*) Difference profiles showing the transbilayer distribution of the deuterated F384 and L385 in wild-type. The experimental difference profile (*thick dotted line*), with a maximum at the bilayer center, is the envelope of two distributions centered at $Z_{D(FL)}$ close to the bilayer center (*dashed lines*). Multiple pairs of Gaussian parameters {position ($Z_{D(FL)}$), width ($A_{D(FL)}$)} (compare panels *B* and *C*) produce fits that are consistent with the data ($R_{fit} < R_{self}$), such that exact values of $Z_{D(FL)}$ and $A_{D(FL)}$ cannot be calculated. In panels *B* and *C*, two possible Gaussian distributions are shown with dashed lines; their envelopes (*solid line*) approximate well the experimental profile (*thick dotted line*). The range of positions and widths that are consistent with the experimental data are $0 \leq Z_{D(FL)} \leq 2.5$ Å and $4 \leq A_{D(FL)} \leq 5.8$ Å.

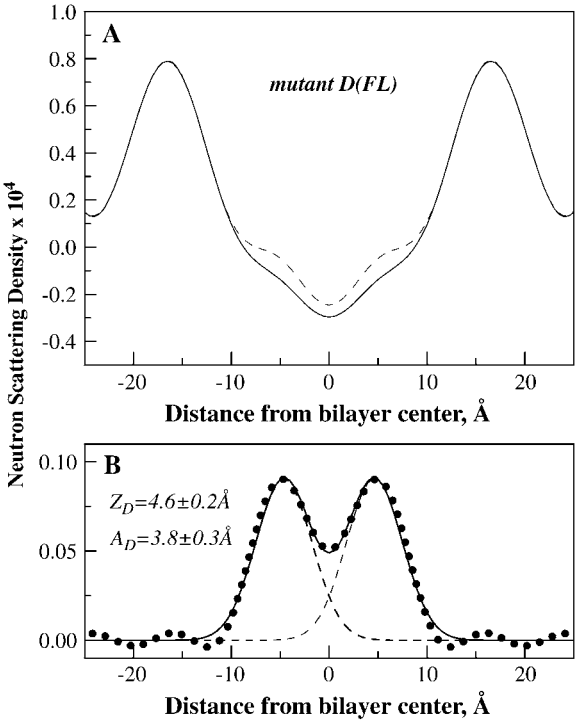

FIGURE 6 (*A*) Absolute neutron scattering length density profiles for bilayers with 4 mol % TM_{mut} and $TM_{mut}^{D(FL)}$. (*B*) Difference profiles, showing the transbilayer distribution of the deuterated F384 and L385 in the mutant. For the mutant, the parameters of the F384/L385 deuterium distribution can be determined with high experimental precision: $Z_{D(FL)} = 4.6 \pm 0.2$ Å, $A_{D(FL)} = 3.8 \pm 0.2$ Å. The experimental difference profile is shown with the thick dotted line, the two F384/L385 Gaussians are shown with the dashed lines, and their envelope is shown with the solid line.

dotted lines), are the envelopes of the two water Gaussians from apposing bilayers.

Topology of the R380 mutant in POPC bilayers

As discussed above, the F384/L385 deuterium label distribution in the mutant is centered at 4.6 Å from the bilayer center (Fig. 6). The center of the membrane-embedded segment, however, cannot be unambiguously determined based solely on this result. For instance, if we assume that the mutant TM domain is normal to the bilayer, which is consistent with the OCD data in Fig. 2, two different topologies would be consistent with a F384/L385 location at 4.6 Å from the bilayer center. In the first case, I387 and L388 are in the middle of the bilayer, while in the second case, R380 is in the middle of the bilayer.

To determine the exact topology of the mutant TM domain, we synthesized a mutant variant $TM_{mut}^{D(LVV)}$ with deuterated L388, V389, and V390 (26 deuterons per peptide) and we determined the position of the deuterium label *D*(*LVV*) within the bilayer thickness. The scaled absolute structure factors are shown in Table 1. Fig. 8 *A* compares the absolute scattering length density profiles of POPC bilayers with 4 mol % TM_{mut} (*solid line*) and $TM_{mut}^{D(LVV)}$ (*dashed line*). The difference between the two profiles in Fig. 8 *A* is due to the isomorphous replacement of 26 hydrogens with deuterons in L388, V389, and V390. Fig. 8, *B* and *C*, show the difference profile (*thick dotted line*), which describes the transbilayer distribution of the *D*(*LVV*) label. The label appears very close to the bilayer center, and, just as in the case of wild-type, multiple pairs of Gaussian distributions are consistent with the

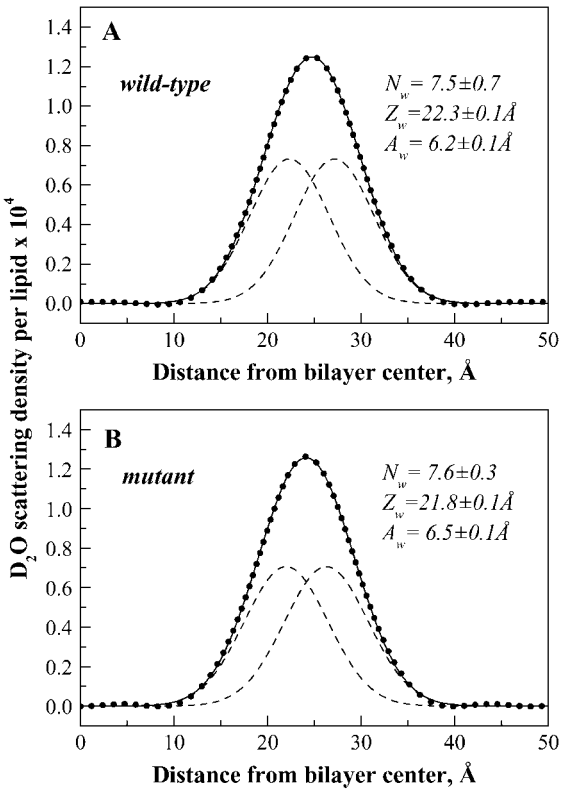

FIGURE 7 Experimental (*thick dotted lines*) and fitted difference profiles describing the water distribution in bilayers with wild-type and mutant FGFR3 TM domains. The fitted water Gaussians, derived from the averaged parameters shown in Table 3, are shown with the dashed lines. The solid lines are the envelopes of the two water Gaussians from apposing bilayers.

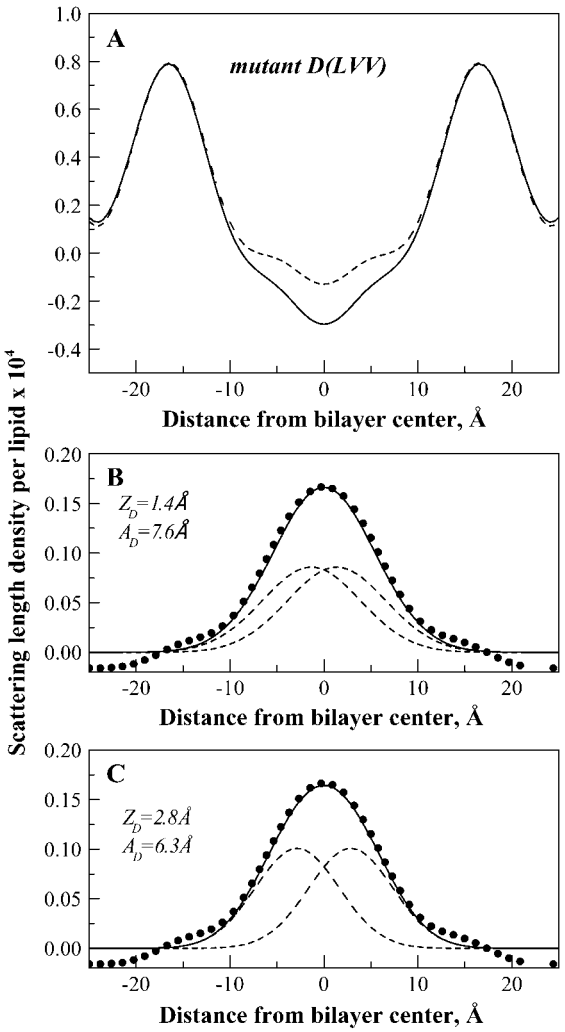

FIGURE 8 (*A*) Absolute neutron scattering length density profiles for bilayers with 4 mol % TM_{mut} and $TM_{mut}^{D(LVV)}$ at 76% RH. The difference between the two profiles is due to the isomorphous replacement of 26 hydrogens in L388, V389, and V390 with 26 deuterons (see Fig. 1). (*B*,*C*) Difference profiles showing the transbilayer distribution of the deuterated L388, V389, and V390 in the mutant. Multiple pairs of Gaussian parameters {position ($Z_{D(LVV)}$), width ($A_{D(LVV)}$)} produce fits that are consistent with the data ($R_{fit} < R_{self}$). The individual deuterium label distributions are shown with dashed lines; their envelopes (*solid line*) approximate well the experimental profile (*thick dotted line*). The range of positions and widths that are consistent with the experimental data are $1.4 \leq Z_{D(LVV)} \leq 2.8$ Å and $6.3 \leq A_{D(LVV)} \leq 7.8$ Å.

experimental data. In particular, distributions centered in the range 1.4–2.8Å are all consistent with the data, i.e., $R_{fit} < R_{self}$. Since three consecutive amino acids, 388–390, were deuterated, the center of the distribution, at ~2 Å from the bilayer center, points to the position of V389 within the bilayer thickness.

Thus, we find that the *D*(*FL*) distribution for the mutant is centered at 4.6 Å from the bilayer center, while the position of *D*(*LVV*) and therefore, V389, is between 1.4 and 2.8 Å. These values could be used to gain information about the disposition of the helix in the bilayer, if we assume that no kinks exist in the hydrocarbon-core embedded segments. Such an assumption could be justified, since hydrogen bonds confer stability on TM helices (3), and kinks will likely perturb the hydrogen-bond network and destabilize the TM helices.

If the two labels, *D*(*FL*) and *D*(*LVV*), are positioned within the same bilayer leaflet, the difference in their depth of penetration would be only ~2–3 Å. This would imply that the TM domain is tilted with respect to the bilayer normal (see Fig. 9 *A*). The tilt, expected to be between 60 and 74°, is inconsistent with the OCD data, shown in Fig. 2.

If the two deuterium labels, *D*(*FL*) and *D*(*LVV*), are on the opposite sides of the midbilayer plane, the distance between them would be between 6 and 7.4 Å. On the other hand, assuming that the rise per residue in the helix is 1.5 Å, the distance between the two labels along the helix axis can be calculated as 6.75 Å. Therefore, the helix tilt in this case would be between 0 and 27° (Fig. 9 *B*), in agreement with the OCD data.

The above reasoning leads us to conclude that the two labels, *D*(*FL*) and *D*(*LVV*), are on opposite sides of the bilayer center. The position of the *D*(*FL*) label is known exactly, at 4.6 Å from the bilayer center. The helix tilt, as determined by OCD, is between 0 and 20° with respect to the bilayer normal. Although the exact tilt angle is unknown, the depth of penetration of various amino acids in the hydrocarbon core can be determined

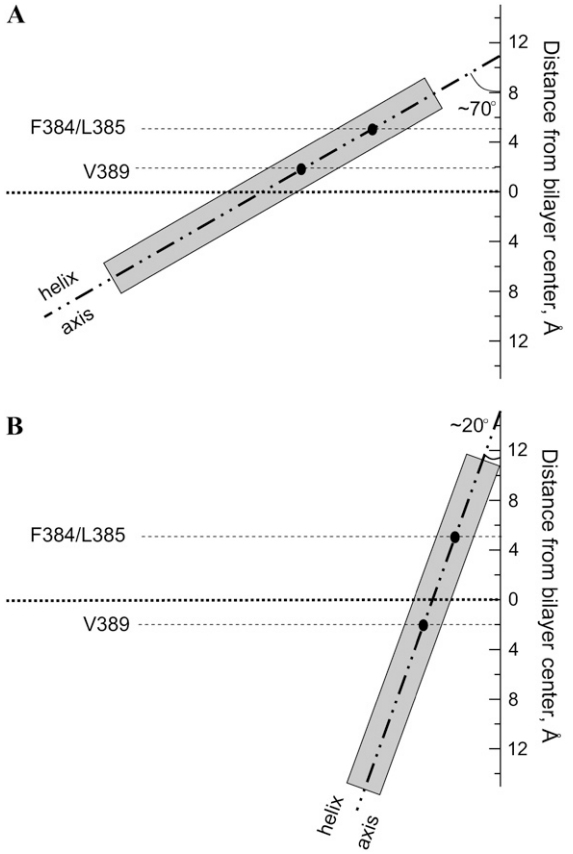

FIGURE 9 (*A*) If the two deuterium labels, *D*(*FL*) and *D*(*LVV*), are positioned within the same bilayer leaflet, the difference in their depth of penetration would be only ~2–3 Å. Therefore, the FGFR3 TM helix would be tilted. The tilt, expected to be between 60 and 74°, is inconsistent with the OCD data, shown in Fig. 2. (*B*) If the two deuterium labels, *D*(*FL*) and *D*(*LVV*), are on the opposite sides of the midbilayer plane, the tilt is <27°, consistent with the OCD data.

(Fig. 10). The midpoint of the mutant TM FGFR3 domain is between I387 and L388, and R380 is at ~11 Å from the bilayer center (Fig. 10). Therefore, the experimental data do not support the hydropathy analysis prediction that V381 in the mutant is located in the middle of the bilayer.

DISCUSSION

Neutron diffraction studies of depth of penetration of amino acids in fluid bilayers

Neutron diffraction experiments, combined with specific deuteration of amino acids, offer a means to determine the depth of penetration of the deuterated amino acids within the bilayer thickness. Here we have verified this approach by demonstrating that the hydrogen-deuterium substitution in a TM domain is indeed an isomorphous replacement that introduces no perturbations in the bilayer structure, as evident from the complete overlap of profiles away from the labels in Figs. 5 *A*, 6 *A*, and 8 *A*.

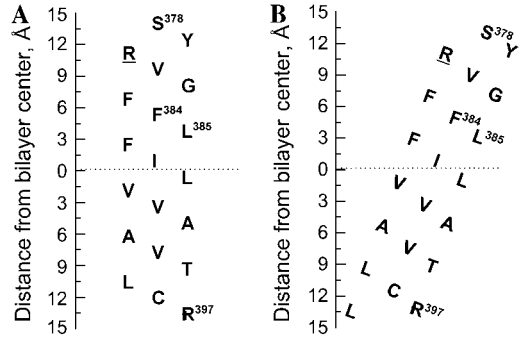

FIGURE 10 Sketch of the hydrocarbon core-embedded segment of the G380R mutant, which is consistent with the neutron diffraction and OCD data. The tilt of the helix, based on the OCD data, is between 0 and 20° with respect to the bilayer normal. The position of the F384/L385 label is at 4.6 Å from the bilayer center, and V389 is positioned within the opposite bilayer leaflet. (*A*) Tilt angle = 0°. R380 (*underlined*) is located at ~11 Å from the bilayer center, while R397 is at ~14 Å from the bilayer center. This structural picture is consistent with work by Hessa et al. (4), who showed that arginine is well tolerated at the periphery of the hydrocarbon core region, but not in the center of the bilayer. (*B*) Tilt angle = 20°. R380 (*underlined*) is located at ~11 Å from the bilayer center, while R397 is at ~13 Å from the bilayer center. Although the exact tilt of the helix is not known, the depth of penetration of the amino acids in the hydrocarbon core can be determined, assuming that there are no kinks in the helix.

A crucial issue for the feasibility of neutron diffraction experiments that locate amino acids within the bilayer thickness is the detection limit for deuterium (i.e., the number of deuterons per lipid that can be detected), as determined by the number of deuterons per peptide and the peptide/lipid ratio. In the present experimental study, we introduced at least 0.625 deuterons per lipid, and we showed that these 0.625 deuterons provide sufficient contrast, such that the position of the deuterons within the bilayer can be resolved. This conclusion is supported by comparing values of R_{self}, measuring the quality of the data, and R_{diff}, reporting the difference in structure factors due to the presence of the deuterium label. As shown in Tables 2 and 3, the values of R_{diff} in our experiments exceed the values of R_{self} two-to-threefold, such that the contrast introduced by the specific

TABLE 2 Gaussian parameters for the *D*(*FL*) and *D*(*LVV*) deuterium distributions in POPC bilayers containing 4 mol % wild-type or mutant TM domains

	Wild-type *D*(*FL*)	Mutant *D*(*FL*)	Mutant *D*(*LVV*)
Z_D (Å)*	$0 \le Z_D \le 2.5$	4.6 ± 0.2	$1.4 \le Z_D \le 2.8$
A_D (Å)†	$4.0 \le A_D \le 5.8$	3.8 ± 0.3	$6.3 \le A_D \le 7.5$
R_{diff}‡	0.099	0.099	0.123
R_{fit}§	0.011–0.013	0.016	0.021–0.023

*Center of the deuterium distribution.
†Width of the deuterium distribution.
‡Difference *R*-factor, $R_{diff} = \sum_{h=1}^{h_{obs}} |(F(h) - F^D(h))| / \sum_{h=1}^{h_{obs}} |F(h)|$, where $F(h)$ and $F^D(h)$ are the structure factors in the absence and presence of the peptide deuterium label, either *D*(*FL*) or *D*(*LVV*); see text. The transbilayer distribution of the deuterium label can be determined only if $R_{diff} > R_{self}$.
§*R*-factor for the fit, $R_{fit} = \sum_{h=1}^{h_{obs}} |(F - F_{fit})(h)| / \sum_{h=1}^{h_{obs}} |F(h)|$.

TABLE 3 Gaussian parameters for the water distributions

	TM_{wt}	$TM_{wt}^{D(FL)}$	$WT_{average}$¶	TM_{mut}	$TM_{mut}^{D(FL)}$	$MUT_{average}$‖
Z_w (Å)*	22.4 ± 0.1	22.2 ± 0.1	22.3 ± 0.1	22.1 ± 0.1	21.6 ± 0.1	21.8 ± 0.1
A_w (Å)†	6.1 ± 0.1	6.2 ± 0.1	6.2 ± 0.1	6.5 ± 0.2	6.4 ± 0.2	6.5 ± 0.1
N_w‡	8.0 ± 0.3	6.9 ± 0.1	7.5 ± 0.7	7.6 ± 0.3	7.6 ± 0.4	7.6 ± 0.3
R_{fit}§	0.0056	0.0133		0.0061	0.0069	

*Center of water distribution.
†Width of water distribution.
‡Number of water molecules per lipid.
§R-factor for the water fit, $R_{fit} = \sum_{h=1}^{h_{obs}} |(F - F_{fit})(h)| / \sum_{h=1}^{h_{obs}} |F(h)|$. For a good fit, $R_{fit} < R_{self}$ (R_{self} defined in Table 1).
¶Averaged values for TM_{wt} and $TM_{wt}^{D(FL)}$.
‖Averaged values for TM_{mut} and $TM_{mut}^{D(FL)}$.

deuteration is not ''hidden'' within the experimental noise. Comparison between values of R_{diff} and R_{self} should be always carried out in similar experiments. If $R_{diff} \leq R_{self}$, the differences in structure factors due to the label will be similar to the experimental noise, and the position of the deuterium label cannot be determined. Given the values of R_{self} and R_{diff} in our experiments, it appears that the detection of $<\sim 0.6$ deuterons per lipid is problematic. However, as long as there are >0.6 deuterons per lipid, neutron diffraction provides a direct means to determine the depth of penetration of amino acids in bilayers.

The achondroplasia mutation does not induce a major change in membrane topology

Oriented CD experiments show that the wild-type and the mutant adopt transmembrane orientations, characterized by low tilt ($<20°$) with respect to the bilayer normal. Thus, Arg^{380} inserts into the bilayer, and does not cause a major change in bilayer topology.

Previous work has shown that the two peptides have similar dimerization propensities in lipid bilayers (22), and therefore similar distributions of monomers and dimers at each peptide concentration. Based on measured dimerization equilibrium constants (22), both peptides are expected to be predominantly in the dimeric state at the concentration used in the neutron diffraction experiments ($\sim$70% in the dimeric state). Molecular modeling of the wild-type dimer (20) predicts a crossing angle between helices of $\sim$17°, suggesting that the helix tilt in the dimeric state is 8.5° with respect to the bilayer normal. This prediction is within the experimentally determined tilts of 20° or less for both wild-type and mutant. We note that the tilt of the monomeric and dimeric peptides may differ, and the experiments may report the average value. Furthermore, we note that variations in tilt between 0 and 20° cannot be detected by either OCD or diffraction, as illustrated in Figs. 2 and 10.

Structural consequences of the achondroplasia mutation

The results obtained in this article allow us to compare directly the structural parameters of bilayers with 4 mol % wild-type FGFR3 TM domain and the achondroplasia-causing R380 mutant. The first obvious difference between bilayers with wild-type and mutant TM domains is their Bragg spacings. The Bragg spacing reports the thickness of the unit cell, and thus the thickness of the bilayer containing the peptides plus the associated water. The Bragg spacing is $\sim$49.5 Å in the presence of wild-type and $\sim$48.5 Å in the presence of the mutant. The decrease of $\sim$1 Å is small, yet significant.

The measured structure factors in Table 1 are on the absolute scale, such that they can be directly compared. We see slight, but significant differences between structure factors of bilayers with wild-type and mutant TM domains. Furthermore, the depth of penetration of the deuterium F384/L385 label into the bilayer is also different for the wild-type and the mutant. The position of the label is between 0 and 2.5 Å for wild-type and 4.6 Å for the mutant. While G380 in wild-type is positioned at $\sim$6 Å from the bilayer center, the mutant R380 is at $\sim$11 Å from the bilayer center. Thus, it appears that the achondroplasia mutation induces a shift in the membrane-embedded segment of FGFR3. The shift, induced by R380, brings R397 inside the hydrocarbon core, at $\sim$13–14 Å from the bilayer center (see Fig. 10). This structural picture is consistent with work by Hessa et al. (4), who showed that arginine is well tolerated at the periphery of the hydrocarbon core region, but not in the center of the bilayer. It should be further noted that hydropathy analysis tools do not predict correctly the location of R380, and the overall topology of FGFR3 TM domain in the bilayer.

Unlike the other structural parameters, the transbilayer distribution of the water, uptaken by bilayers with wild-type and mutant proteins, appears very similar. Thus, the R380 mutation does not affect the water uptake by the bilayer.

Mechanism of pathogenesis in achondroplasia

The G380R mutation in FGFR3 TM domain causes achondroplasia, an autosomal dominant disorder that affects the maturation of the cartilage growth plate of long bones (24). The underlying cellular basis of the disorder is a defect in chondrocyte function during endochondral bone formation.

The molecular mechanism of pathology induction is under debate, and two different mechanisms have been proposed to contribute to pathogenesis: 1), R380-mediated FGFR3 dimer stabilization (19); and 2), slow downregulation of the activated mutant receptors (29,30). We have previously reported that the mutation does not alter the stability of the FGFR3 TM domain dimer (22), and thus the phenotypic changes cannot be described simply by enhanced dimer stability.

Monsonego-Ornan and colleagues (29) have shown that the activated G380R receptors accumulate in the plasma membrane because they are downregulated very slowly. Cho et al. (28) have demonstrated that the mutant receptors escape lysosomal degradation and are recycled back to the plasma membrane, thus prolonging signaling. Our previous finding that the mutation does not stabilize the FGFR3 TM dimer (22) emphasizes the importance of the observed slow downregulation of the mutant receptor in achondroplasia. The exact mechanism of the slow downregulation, however, is unknown. Here we observe structural changes as a consequence of the R380 mutation: in a model system, the mutation induces a decrease in Bragg spacing and a shift in the membrane-embedded segment. It is possible that the observed structural changes play a role in pathogenesis in achondroplasia. For instance, the basis of the compromised downregulation of the mutant receptor could be structural.

We thank Drs. U. Perez-Salas and D. Worcester for their help with neutron data collection and processing, and for useful discussions.

This work was supported by National Institutes of Health grant No. GM 068619. We acknowledge the support of the National Institute of Standards and Technology, U.S. Department of Commerce and the Cold Neutrons for Biology and Technology program funded by the National Institutes of Health under grant No. RR1481-2 and the Regents of the University of California.

REFERENCES

1. White, S. H., and W. C. Wimley. 1999. Membrane protein folding and stability: physical principles. *Annu. Rev. Biophys. Biomol. Struct.* 28: 319–365.
2. White, S. H., W. C. Wimley, A. S. Ladokhin, and K. Hristova. 1998. Protein folding in membranes: pondering the nature of the bilayer milieu. *Biol. Skr. Dan. Selsk.* 49:91–98.
3. Jayasinghe, S., K. Hristova, and S. H. White. 2001. Energetics, stability, and prediction of transmembrane helices. *J. Mol. Biol.* 312: 927–934.
4. Hessa, T., S. H. White, and G. von Heijne. 2005. Membrane insertion of a potassium-channel voltage sensor. *Science*. 307:1427.
5. Hessa, T., H. Kim, K. Bihlmaier, C. Lundin, J. Boekel, H. Andersson, I. Nilsson, S. H. White, and G. von Heijne. 2005. Recognition of transmembrane helices by the endoplasmic reticulum translocon. *Nature*. 433:377–381.
6. Abrams, F. S., and E. London. 1993. Extension of the parallax analysis of membrane penetration depth to the polar region of model membranes: use of fluorescence quenching by a spin-label attached to the phospholipid polar headgroup. *Biochemistry*. 32:10826–10831.
7. Kachel, K., E. Asuncion-Punzalan, and E. London. 1995. Anchoring of tryptophan and tyrosine analogs at the hydrocarbon-polar boundary in model membrane vesicles: parallax analysis of fluorescence quenching induced by nitroxide-labeled phospholipids. *Biochemistry*. 34:15475–15479.
8. London, E., and A. S. Ladokhin. 2001. Measuring the depth of membrane penetration by amino acid residues in peptides using fluorescence quenching. *In* Peptide-Lipid Interactions. S. A. Simon and T. J. McIntosh, editors. Academic Press, New York.
9. Macosko, J. C., C.-H. Kim, and Y.-K. Shin. 1997. The membrane topology of the fusion peptide region of influenza hemagglutinin determined by spin-labeling EPR. *J. Mol. Biol.* 267:1139–1148.
10. Hubbell, W. L., and C. Altenbach. 1994. Investigation of structure and dynamics in membrane proteins using site-directed spin labeling. *Curr. Opinion Struct. Biol.* 4:566–573.
11. Greenhalgh, D. A., C. Altenbach, W. L. Hubbell, and H. G. Khorana. 1991. Locations of Arg-82, Asp-85, and Asp-96 in helix C of bacteriorhodopsin relative to the aqueous boundaries. *Proc. Natl. Acad. Sci. USA*. 88:8626–8630.
12. Altenbach, C., W. Froncisz, J. S. Hyde, and W. L. Hubbell. 1989. Conformation of spin-labeled melittin at membrane surfaces investigated by pulse saturation recovery and continuous wave power saturation electron paramagnetic resonance. *Biophys. J.* 56:1183–1191.
13. Bradshaw, J. P., M. J. M. Darkes, T. A. Harroun, J. Katsaras, and R. M. Epand. 2000. Oblique membrane insertion of viral fusion peptide probed by neutron diffraction. *Biochemistry*. 39:6581–6585.
14. Dante, S., T. Hauss, and N. A. Dencher. 2002. β-amyloid 25 to 35 is intercalated in anionic and zwitterionic lipid membranes to different extents. *Biophys. J.* 83:2610–2616.
15. Hauss, T., S. Dante, T. H. Haines, and N. A. Dencher. 2005. Localization of coenzyme Q(10) in the center of a deuterated lipid membrane by neutron diffraction. *Biochim. Biophys. Acta Bioenerg.* 1710:57–62.
16. Bradshaw, J. P., M. J. M. Darkes, J. Katsaras, and R. M. Epand. 2000. Neutron diffraction studies of viral fusion peptides. *Physica B (Amsterdam)*. 276:495–498.
17. Wiener, M. C., and S. H. White. 1991. Transbilayer distribution of bromine in fluid bilayers containing a specifically brominated analog of dioleoylphosphatidylcholine. *Biochemistry*. 30:6997–7008.
18. Li, E., M. You, and K. Hristova. 2005. SDS-PAGE and FRET suggest weak interactions between FGFR3 TM domains in the absence of extracellular domains and ligands. *Biochemistry*. 44:352–360.
19. Webster, M. K., and D. J. Donoghue. 1996. Constitutive activation of fibroblast growth factor receptor 3 by the transmembrane domain point mutation found in achondroplasia. *EMBO J.* 15:520–527.
20. Li, E., M. You, and K. Hristova. 2006. FGFR3 dimer stabilization due to a single amino acid pathogenic mutation. *J. Mol. Biol.* 356: 600–612.
21. Merzlyakov, M., M. You, E. Li, and K. Hristova. 2006. Transmembrane helix heterodimerization in lipids bilayers: probing the energetics behind autosomal dominant growth disorders. *J. Mol. Biol.* 358:1–7.
22. You, M., E. Li, and K. Hristova. 2006. The achondroplasia mutation does not alter the dimerization energetics of FGFR3 transmembrane domain. *Biochemistry*. 45:5551–5556.
23. van Rhijin, B., A. van Tilborg, I. Lurkin, J. Bonaventure, A. de Vries, J. P. Thiery, T. H. van der Kwast, E. Zwarthoff, and F. Radvanyi. 2002. Novel fibroblast growth factor receptor 3 (FGFR3) mutations in bladder cancer previously identified in non-lethal skeletal disorders. *Eur. J. Hum. Genet.* 10:819–824.
24. Vajo, Z., C. A. Francomano, and D. J. Wilkin. 2000. The molecular and genetic basis of fibroblast growth factor receptor 3 disorders: the achondroplasia family of skeletal dysplasias, Muenke craniosynostosis, and Crouzon syndrome with *Acanthosis nigricans*. *Endocr. Rev.* 21: 23–39.
25. Shiang, R., L. M. Thompson, Y.-Z. Zhu, D. M. Church, T. J. Fielder, M. Bocian, S. T. Winokur, and J. J. Wasmuth. 1994. Mutations in the transmembrane domain of FGFR3 cause the most common genetic form of dwarfism, achondroplasia. *Cell*. 78:335–342.

26. Weiner, D. B., J. Liu, J. A. Cohen, W. V. Williams, and M. I. Greene. 1989. A point mutation in the Neu oncogene mimics ligand induction of receptor aggregation. *Nature*. 339:230–231.

27. Li, E., and K. Hristova. 2006. Role of receptor tyrosine kinase transmembrane domains in cell signaling and human pathologies. *Biochemistry*. 45:6241–6251.

28. Cho, J. Y., C. S. Guo, M. Torello, G. P. Lunstrum, T. Iwata, C. X. Deng, and W. A. Horton. 2004. Defective lysosomal targeting of activated fibroblast growth factor receptor 3 in achondroplasia. *Proc. Natl. Acad. Sci. USA*. 101:609–614.

29. Monsonego-Ornan, E., R. Adar, T. Feferman, O. Segev, and A. Yayon. 2000. The transmembrane mutation G380R in fibroblast growth factor receptor 3 uncouples ligand-mediated receptor activation from down-regulation. *Mol. Cell. Biol.* 20:516–522.

30. Monsonego-Ornan, E., R. Adar, E. Rom, and A. Yayon. 2002. FGF receptors ubiquitylation: dependence on tyrosine kinase activity and role in downregulation. *FEBS Lett*. 528:83–89.

31. Wiener, M. C., G. I. King, and S. H. White. 1991. Structure of a fluid dioleoylphosphatidylcholine bilayer determined by joint refinement of x-ray and neutron diffraction data. I. Scaling of neutron data and the distribution of double-bonds and water. *Biophys. J*. 60:568–576.

32. Hristova, K., and S. H. White. 1998. Determination of the hydrocarbon core structure of fluid dioleoylphosphatidylcholine (DOPC) bilayers by x-ray diffraction using specific bromination of the double-bonds: effect of hydration. *Biophys. J*. 74:2419–2433.

33. Jacobs, R. E., and S. H. White. 1989. The nature of the hydrophobic binding of small peptides at the bilayer interface: implications for the insertion of transbilayer helices. *Biochemistry*. 28:3421–3437.

34. Wiener, M. C., and S. H. White. 1992. Structure of a fluid dioleoylphosphatidylcholine bilayer determined by joint refinement of x-ray and neutron diffraction data. III. Complete structure. *Biophys. J*. 61:434–447.

35. Hristova, K., W. C. Wimley, V. K. Mishra, G. M. Anantharamaiah, J. P. Segrest, and S. H. White. 1999. An amphipathic α-helix at a membrane interface: a structural study using a novel x-ray diffraction method. *J. Mol. Biol*. 290:99–117.

36. Hristova, K., C. E. Dempsey, and S. H. White. 2001. Structure, location, and lipid perturbations of melittin at the membrane interface. *Biophys. J*. 80:801–811.

37. Iwamoto, T., M. You, E. Li, J. Spangler, J. M. Tomich, and K. Hristova. 2005. Synthesis and initial characterization of FGFR3 transmembrane domain: consequences of sequence modifications. *Biochim. Biophys. Acta*. 1668:240–247.

38. Li, E., and K. Hristova. 2004. Imaging FRET measurements of transmembrane helix interactions in lipid bilayers on a solid support. *Langmuir*. 20:9053–9060.

39. You, M., E. Li, W. C. Wimley, and K. Hristova. 2005. FRET in liposomes: measurements of TM helix dimerization in the native bilayer environment. *Anal. Biochem*. 340:154–164.

40. Vogel, H. 1987. Comparison of the conformation and orientation of alamethicin and melittin in lipid membranes. *Biochemistry*. 26: 4562–4572.

41. Olah, G. A., and H. W. Huang. 1988. Circular dichroism of oriented α-helices. I. Proof of the exciton theory. *J. Chem. Phys*. 89:2531–2538.

42. Olah, G. A., and H. W. Huang. 1988. Circular dichroism of oriented α-helices. II. Electric field oriented polypeptides. *J. Chem. Phys*. 89: 6956–6962.

43. Worcester, D. L., and N. P. Franks. 1976. Structural analysis of hydrated egg lecithin and cholesterol bilayers. II. Neutron diffraction. *J. Mol. Biol*. 100:359–378.